

Nuclear Magnetic Relaxation Rate in a Noncentrosymmetric Superconductor

N. Hayashi,¹ K. Wakabayashi,^{1,2} P. A. Frigeri,¹ and M. Sgrist¹

¹ *Institut für Theoretische Physik, ETH-Hönggerberg, CH-8093 Zürich, Switzerland*

² *Department of Quantum Matter Science, Graduate School of Advanced Sciences of Matter (ADSM), Hiroshima University, Higashi-Hiroshima 739-8530, Japan*

(Dated: March 23, 2022)

For a noncentrosymmetric superconductor such as CePt₃Si, we consider a Cooper pairing model with a two-component order parameter composed of spin-singlet and spin-triplet pairing components. We demonstrate that such a model on a qualitative level accounts for experimentally observed features of the temperature dependence of the nuclear spin-lattice relaxation rate T_1^{-1} , namely a peak just below T_c and a line-node gap behavior at low temperatures.

Inversion symmetry is one of the key points for the formation of Cooper pairs in superconductors. Unusual properties arise in superconductors whose crystal structure does not possess an inversion center (*e.g.*, Refs. [1, 2, 3, 4, 5], and references therein). The recent discovery of superconductivity in the noncentrosymmetric heavy Fermion compound CePt₃Si has initiated much interest, as experimental data revealed various intriguing features [6, 7, 8]. The essential element in modelling noncentrosymmetric systems is the presence of antisymmetric spin-orbit coupling [9, 10]. One of the characteristic features in the superconducting phase is the mixing of the spin-singlet and spin-triplet Cooper pairing channels which are otherwise distinguished by parity [2]. This is likely responsible for the surprisingly high value of the upper critical field H_{c2} which exceeds the paramagnetic limit [3, 6, 8, 11, 12]. CePt₃Si displays further intriguing properties. Recent nuclear magnetic resonance (NMR) experiments found an overall anomalous temperature dependence of the nuclear spin-lattice relaxation rate T_1^{-1} [8, 13, 14]. The behavior of T_1^{-1} shows a (Hebel-Slichter) peak just below the superconducting critical temperature T_c , and simultaneously a T^3 dependence at low temperatures indicating line nodes in the quasiparticle gap. Such a gap with line nodes is also suggested by measurements of the London penetration depth [8]. At first sight, those experimental results seem to be mutually contradicting, as the features of unconventional Cooper pairing (line nodes) and of conventional superconductivity (peak in T_1^{-1} due to the coherence effect) are implied at the same time by the temperature dependence of T_1^{-1} [8, 13, 14].

In the present study, we demonstrate that these apparently conflicting behaviors can be reconciled by taking account of the mixing of the pairing channels with opposite parity, which naturally occurs in superconductors without inversion center. For this purpose, we consider a pairing model with a two-component order parameter consisting of spin-singlet and spin-triplet pairing components. Such a model contains the necessary ingredients to account for the observed features of T_1^{-1} , i.e., the line-node behavior at low temperatures and the coherence effect just below T_c . At the same time, the pairing model

would also explain the temperature dependence of the London penetration depth qualitatively and be consistent with earlier studies of H_{c2} [3, 15].

We base our analysis on a Hamiltonian considered in Ref. [3], in which the lack of inversion symmetry is incorporated through the antisymmetric spin-orbit coupling [3, 12, 16]

$$\alpha \mathbf{g}_k \cdot \mathbf{S} \quad \text{with} \quad \mathbf{g}_k = \sqrt{\frac{3}{2}}(-\tilde{k}_y, \tilde{k}_x, 0). \quad (1)$$

Here, \mathbf{S} is the electron spin operator, α (> 0) denotes the strength of the spin-orbit coupling, the vector \mathbf{g}_k ($\mathbf{g}_{-k} = -\mathbf{g}_k$) is determined by symmetry arguments, and $\tilde{\mathbf{k}} = (\tilde{k}_x, \tilde{k}_y, \tilde{k}_z) = (\cos \phi \sin \theta, \sin \phi \sin \theta, \cos \theta)$.

Starting from the tetragonal symmetry of CePt₃Si, it is possible to classify the basic pairing states, distinguishing the spin-singlet and spin-triplet states [3, 5]. The general argument by Anderson [17] shows that the inversion symmetry is a key element for the realization of spin-triplet pairing. Hence, turning on antisymmetric spin-orbit coupling would be detrimental for spin-triplet pairing. The detailed examination of this aspect, however, led to the conclusion that among the spin-triplet states, only the \mathbf{d} vector parallel to \mathbf{g}_k , [$\mathbf{d}_k \parallel (-\tilde{k}_y, \tilde{k}_x, 0)$], is robust against this symmetry reduction effect of the spin-orbit coupling [3]. Moreover, the antisymmetric spin-orbit coupling mixes spin-singlet and spin-triplet pairings. Interestingly, the conventional *s*-wave spin-singlet pairing state mixes precisely with the state corresponding to $\mathbf{d}_k \parallel \mathbf{g}_k$ [16], which will be essential for our discussion.

We consider a superconducting gap function in the following mixing form,

$$\begin{aligned} \hat{\Delta}_k &= (\Psi \hat{\sigma}_0 + \mathbf{d}_k \cdot \hat{\boldsymbol{\sigma}}) i \hat{\sigma}_y \\ &= \left[\Psi \hat{\sigma}_0 + \Delta(-\tilde{k}_y \hat{\sigma}_x + \tilde{k}_x \hat{\sigma}_y) \right] i \hat{\sigma}_y, \end{aligned} \quad (2)$$

with the *s*-wave pairing component Ψ and the \mathbf{d} vector $\mathbf{d}_k = \Delta(-\tilde{k}_y, \tilde{k}_x, 0)$. While the spin-triplet part has point nodes, this pairing state can possess line nodes in a gap as a result of the combination with the *s*-wave component. In this paper, we adopt the isotropic *s*-wave pairing as Ψ for simplicity.

We will discuss the superconducting phase by means of the quasiclassical theory of superconductivity [18, 19, 20].

The quasiclassical Green function \check{g} is written as a matrix in Nambu (particle-hole) space,

$$\check{g}(\mathbf{r}, \tilde{\mathbf{k}}, i\omega_n) = -i\pi \begin{pmatrix} \hat{g} & i\hat{f} \\ -i\hat{f} & -\hat{g} \end{pmatrix}. \quad (3)$$

The vector \mathbf{r} is the real-space coordinates, the unit vector $\tilde{\mathbf{k}}$ indicates the position on the Fermi surface, and $\omega_n = \pi T(2n+1)$ is the Matsubara frequency. Throughout the paper, “*hat*” $\hat{\bullet}$ denotes the 2×2 matrix in the spin space, and “*check*” $\check{\bullet}$ denotes the 4×4 matrix composed of the 2×2 Nambu space and the 2×2 spin space. The Eilenberger equation which includes the spin-orbit coupling [Eq. (1)] is given by [21, 22, 23, 24]

$$i\mathbf{v}_F \cdot \nabla \check{g} + [i\omega_n \check{\tau}_3 - \alpha \check{\mathbf{g}}_k \cdot \check{\mathbf{S}} - \check{\Delta}_k, \check{g}] = 0, \quad (4)$$

with

$$\check{\tau}_3 = \begin{pmatrix} \hat{\sigma}_0 & 0 \\ 0 & -\hat{\sigma}_0 \end{pmatrix}, \quad \hat{\sigma}_0 = \begin{pmatrix} 1 & 0 \\ 0 & 1 \end{pmatrix}, \quad (5)$$

$$\check{\mathbf{S}} = \begin{pmatrix} \hat{\boldsymbol{\sigma}} & 0 \\ 0 & \hat{\boldsymbol{\sigma}}^{tr} \end{pmatrix}, \quad \hat{\boldsymbol{\sigma}}^{tr} = -\hat{\sigma}_y \hat{\boldsymbol{\sigma}} \hat{\sigma}_y, \quad (6)$$

$$\check{\mathbf{g}}_k = \begin{pmatrix} \mathbf{g}_k \hat{\sigma}_0 & 0 \\ 0 & \mathbf{g}_{-k} \hat{\sigma}_0 \end{pmatrix} = \begin{pmatrix} \mathbf{g}_k \hat{\sigma}_0 & 0 \\ 0 & -\mathbf{g}_k \hat{\sigma}_0 \end{pmatrix}, \quad (7)$$

$$\check{\Delta}_k = \begin{pmatrix} 0 & \hat{\Delta}_k \\ -\hat{\Delta}_k^\dagger & 0 \end{pmatrix}. \quad (8)$$

Here, $\hat{\boldsymbol{\sigma}} = (\hat{\sigma}_x, \hat{\sigma}_y, \hat{\sigma}_z)$ is the Pauli matrix, \mathbf{v}_F is the Fermi velocity, and $[\hat{a}, \hat{b}] = \hat{a}\hat{b} - \hat{b}\hat{a}$. We use units in which $\hbar = k_B = 1$. The Eilenberger equation is supplemented by the normalization condition, $\check{g}^2 = -\pi^2 \check{1}$ [18, 21].

For the pairing state [Eq. (2)], we obtain the following Green functions in the case of spatially uniform system,

$$\hat{g} = g_I \hat{\sigma}_I + g_{II} \hat{\sigma}_{II}, \quad (9a)$$

$$\hat{f} = (f_I \hat{\sigma}_I + f_{II} \hat{\sigma}_{II}) i \hat{\sigma}_y, \quad (9b)$$

$$\hat{\bar{f}} = -i \hat{\sigma}_y (\bar{f}_I \hat{\sigma}_I + \bar{f}_{II} \hat{\sigma}_{II}), \quad (9c)$$

$$\hat{\bar{g}} = -\hat{\sigma}_y (\bar{g}_I \hat{\sigma}_I + \bar{g}_{II} \hat{\sigma}_{II}) \hat{\sigma}_y, \quad (9d)$$

with the matrices $\hat{\sigma}_{I,II}$ defined by [1, 16, 25]

$$\hat{\sigma}_{I,II} = \frac{1}{2} (\hat{\sigma}_0 \pm \bar{\mathbf{g}}_k \cdot \hat{\boldsymbol{\sigma}}), \quad \bar{\mathbf{g}}_k = (-\bar{k}_y, \bar{k}_x, 0). \quad (10)$$

Here, $\bar{\mathbf{k}} = (\bar{k}_x, \bar{k}_y, 0) = (\cos \phi, \sin \phi, 0)$, and

$$g_I = \frac{\omega_n}{B_I}, \quad g_{II} = \frac{\omega_n}{B_{II}}, \quad (11a)$$

$$f_I = \frac{\Psi + \Delta \sin \theta}{B_I}, \quad f_{II} = \frac{\Psi - \Delta \sin \theta}{B_{II}}, \quad (11b)$$

$$\bar{f}_I = \frac{\Psi^* + \Delta^* \sin \theta}{B_I}, \quad \bar{f}_{II} = \frac{\Psi^* - \Delta^* \sin \theta}{B_{II}}, \quad (11c)$$

$$\bar{g}_I = \frac{-\omega_n}{B_I}, \quad \bar{g}_{II} = \frac{-\omega_n}{B_{II}}. \quad (11d)$$

The denominators $B_{I,II}$ are given as

$$B_{I,II} = \sqrt{\omega_n^2 + |\Psi \pm \Delta \sin \theta|^2}, \quad (12)$$

and the signs in front of the square root are determined by the condition, $\text{sgn}(\text{Re}\{g_{I,II}\}) = \text{sgn}(\text{Re}\{\omega_n\})$. Note that the Green functions [Eq. (11)] do not explicitly depend on the spin-orbit coupling constant α . This result of the Eilenberger equation reflects the fact that the spin-triplet component contained in the pairing state [Eq. (2)] is not affected by the antisymmetric spin-orbit coupling of Eq. (1) [3].

The above Green functions labeled by the indices I, II belong to the two distinct Fermi surfaces which are split by the spin-degeneracy lifting due to the spin-orbit coupling $\alpha \mathbf{g}_k \cdot \mathbf{S}$ [1, 16, 25]. While in general the density of states on the two Fermi surfaces is different, we assume that the difference is small and ignore it here.

The pairing interaction leading to the gap function [Eq. (2)] can be characterized by three coupling constants, λ_s , λ_t , and λ_m . Here, λ_s and λ_t result from the pairing interaction within each spin channel (s : singlet, t : triplet). λ_m appears as a scattering of Cooper pairs between the two channels, which is allowed in a system without inversion symmetry [16]. The gap equations are written as

$$\Psi = \lambda_s \pi T \sum_{|\omega_n| < \omega_c} \langle f_+ \rangle + \lambda_m \pi T \sum_{|\omega_n| < \omega_c} \langle \sin \theta f_- \rangle, \quad (13)$$

$$\Delta = \lambda_t \pi T \sum_{|\omega_n| < \omega_c} \langle \sin \theta f_- \rangle + \lambda_m \pi T \sum_{|\omega_n| < \omega_c} \langle f_+ \rangle, \quad (14)$$

where $f_{\pm} = (f_I \pm f_{II})/2$, and ω_c is the cutoff energy. The brackets $\langle \dots \rangle$ denote the average over the Fermi surface. We assume here the spherical Fermi surface for simplicity. In the limit $T \rightarrow T_c$, the linearized gap equations allow us to determine λ_t and λ_s by

$$\lambda_t = \frac{3}{2} \left(\frac{1}{w} - \nu \lambda_m \right), \quad \lambda_s = \frac{2}{3} \lambda_t + \left(\nu - \frac{2}{3\nu} \right) \lambda_m, \quad (15)$$

$$w = \ln \left(\frac{T}{T_c} \right) + \sum_{0 \leq n < (\omega_c / \pi T - 1)/2} \frac{2}{2n+1}, \quad (16)$$

$$\nu = \frac{\Psi}{\Delta} \bigg|_{T \rightarrow T_c}, \quad (17)$$

if the parameters λ_m and ν are given.

In Fig. 1, we show the temperature dependence of the order parameters Δ and Ψ obtained from the gap equations [Eqs. (13) and (14)]. We set $\omega_c = 20T_c$, $\lambda_m = 0.12$, and $\nu = 0.5$, yielding $\lambda_t \approx 0.39$ and $\lambda_s \approx 0.16$. When Δ is fixed to be real and positive without loss of generality,

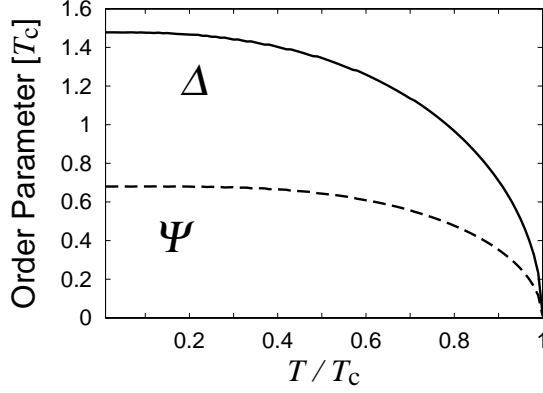


FIG. 1: The temperature dependence of the order parameters in units of T_c . The spin-triplet component Δ (solid line) and the spin-singlet s -wave component Ψ (dashed line). $\omega_c = 20T_c$, $\lambda_m = 0.12$, and $\nu = 0.5$. Both Δ and Ψ are real and positive.

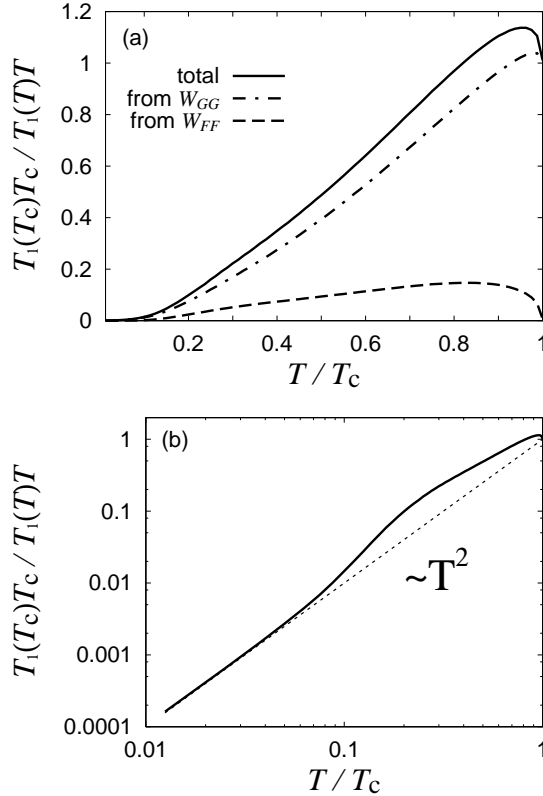


FIG. 2: The temperature dependence of the nuclear spin-lattice relaxation rate $1/T_1T$ (solid lines). $\eta = 10^{-4}T_c$. (a) Dashed line is the contribution of the anomalous Green functions W_{FF} related to the coherence effect. Dash-dotted line is the contribution of the regular Green functions W_{GG} related to the density of states. (b) Plot of the same data on a double-logarithmic scale. Dotted line is a plot of T^2 . From the plot, it is noticed that T_1^{-1} follows the T^3 law at low temperatures.

the solution such that Ψ is also real and positive is stable for the above parameters.

We consider now the nuclear spin-lattice relaxation rate divided by the temperature, $1/T_1T$. Assuming for the NMR experiment a static magnetic field in the z direction, we arrive at the following expression for $1/T_1T$ in terms of the quasiclassical Green function \tilde{g} [26],

$$\frac{T_1(T_c)T_c}{T_1(T)T} = \frac{1}{4T} \int_{-\infty}^{\infty} \frac{d\omega}{\cosh^2(\omega/2T)} W(\omega), \quad (18)$$

with

$$W(\omega) = \langle a_{\downarrow\downarrow}^{22}(\omega) \rangle \langle a_{\uparrow\uparrow}^{11}(-\omega) \rangle - \langle a_{\uparrow\uparrow}^{21}(\omega) \rangle \langle a_{\downarrow\downarrow}^{12}(-\omega) \rangle, \quad (19)$$

$$\tilde{a}(\mathbf{r}, \mathbf{k}, \omega) = \frac{i}{2\pi} \tilde{\tau}_3 \left[\tilde{g}(\mathbf{r}, \mathbf{k}, i\omega_n \rightarrow \omega + i\eta) - \tilde{g}(\mathbf{r}, \mathbf{k}, i\omega_n \rightarrow \omega - i\eta) \right], \quad (20)$$

$$\tilde{a} = \begin{pmatrix} \hat{a}^{11} & \hat{a}^{12} \\ \hat{a}^{21} & \hat{a}^{22} \end{pmatrix}, \quad \hat{a}^{ij} = \begin{pmatrix} a_{\uparrow\uparrow}^{ij} & a_{\uparrow\downarrow}^{ij} \\ a_{\downarrow\uparrow}^{ij} & a_{\downarrow\downarrow}^{ij} \end{pmatrix}, \quad (21)$$

where η (> 0) is an infinitesimally small constant, and we set $\eta = 10^{-4}T_c$.

The temperature dependence of $1/T_1T$ is shown in Fig. 2(a). To obtain it, we used the temperature dependence of Δ and Ψ shown in Fig. 1. Obviously, $1/T_1T$ (solid line) possesses a peak just below T_c . In order to identify the origin of this peak, in Fig. 2(a) we also plot the contributions of the two terms in Eq. (19) separately: $W = W_{GG} + W_{FF}$,

$$W_{GG}(\omega) = \langle a_{\downarrow\downarrow}^{22}(\omega) \rangle \langle a_{\uparrow\uparrow}^{11}(-\omega) \rangle, \quad (22)$$

$$W_{FF}(\omega) = -\langle a_{\uparrow\uparrow}^{21}(\omega) \rangle \langle a_{\downarrow\downarrow}^{12}(-\omega) \rangle. \quad (23)$$

W_{GG} and W_{FF} are composed of the regular Green functions and the anomalous Green functions, respectively. The coherence factor is represented as $1 + W_{FF}/W_{GG}$. The contribution of W_{FF} (dashed line) is related to the coherence effect and gives the dominant contribution to the peak below T_c . In contrast, W_{GG} (dash-dotted line) describes the contribution of the density of states. The contribution to the peak from the singularity of the density of states at the gap edge is minor, since this singularity is rather weak due to the anisotropy of the gaps $|\Psi \pm \Delta \sin \theta|$ on both Fermi surfaces I, II. Note that the anisotropy in the real compound would be enhanced because of the anisotropy of the Fermi surfaces [4]. Therefore, the peak in the total $1/T_1T$ (solid line) can clearly be attributed to the coherence-factor-induced enhancement of the relaxation rate T_1^{-1} originated from the coherence effect.

Turning to the low-temperature behavior, we present the same data on a double-logarithmic scale in Fig. 2(b). The temperature dependence of $1/T_1T$ exhibits a T^2

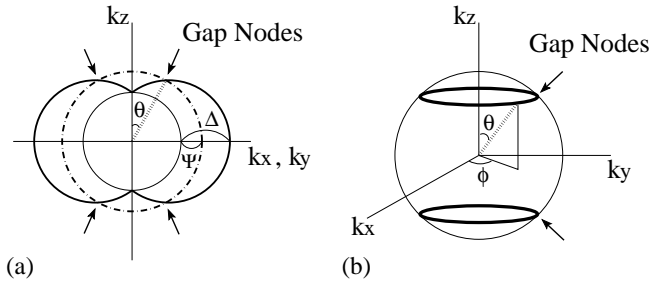


FIG. 3: Schematic figures of the gap structure on the Fermi surface. (a) Cross section of the Fermi surface, showing the places of gap nodes at which the gap $|\Psi - \Delta \sin \theta| = 0$. (b) Line nodes of the gap in the three dimensional \mathbf{k} space.

power law at low temperatures, characteristic of the presence of line nodes in the gap. These nodes are the result from the superposition of spin-singlet and spin-triplet contributions (each separately would not produce line nodes). On the Fermi surface I, the gap is $|\Psi + \Delta \sin \theta|$ and is nodeless, referring to Eq. (11b), (note that $\Psi > 0$, $\Delta > 0$, and $0 \leq \theta \leq \pi$). On the other hand, it has the form $|\Psi - \Delta \sin \theta|$ on the Fermi surface II, where nodes can appear (see Fig. 3). For $|\Psi| \ll |\Delta|$ the gap nodes are located at small θ close to the poles on the Fermi surface, leading to nearly point nodes. With growing s -wave component Ψ , however, the gap nodes move towards the equator of the Fermi surface and form line nodes if $|\Psi| < |\Delta|$, and they disappear if $|\Psi| > |\Delta|$. These line nodes on the Fermi surface II lead to the low-temperature T^3 law in T_1^{-1} (i.e., T^2 in $1/T_1 T$) as shown in Fig. 2(b), which is in qualitative agreement with the experimental result. Moreover, the power law observed in the London penetration depth [8] is also consistent with this explanation.

In conclusion, we identify a natural Cooper pairing state [Eq. (2)] consisting of a spin-singlet s -wave Ψ and a spin-triplet Δ components. This pairing state explains the set of presently available experiments consistently. They include the early experiments on the upper critical field H_{c2} whose behavior can be well explained on the basis of this pairing state [3, 12, 15]. The line nodes which can occur due to the superposition of the two spin channels are very compatible with the observation of the power law behaviors at low temperatures in the London penetration depth and the NMR relaxation rate T_1^{-1} [8, 13, 14]. In addition, this state allows for the Hebel-Slichter coherence peak in T_1^{-1} . It is unlikely that the observed peak could originate from a singularity of the density of states at the gap edge, since such features are most likely washed out by the anisotropy of the quasiparticle gap in the real material. It should also be noted that in CePt_3Si the superconductivity coexists with an antiferromagnetic phase. Muon spin relaxation experiments show that there is little mutual influence of such two orders, suggesting that those two orders might

be associated with different Fermi surfaces respectively [8, 14]. This aspect has to be taken into account when low temperature thermodynamics is analyzed in this material. However, the London penetration depth contains exclusively the information on the superconductivity, and therefore measurements of it [8] belong to the cleanest experiments in probing the gap topology. This fact gives confidence in the existence of line nodes in CePt_3Si .

We thank Y. Kato, J. Goryo, D. F. Agterberg, A. Koga, and M. Matsumoto for helpful discussions. N.H. is supported by 2003 JSPS Postdoctoral Fellowships for Research Abroad. We are also grateful for financial support from the Swiss Nationalfonds and the NCCR MaNEP.

Note added.—After completing this work, we noticed that a similar idea concerning the coexistence between the coherence effect in T_1^{-1} and the line node in a gap was briefly discussed in Ref. [27] by Fujimoto very recently.

-
- [1] V. M. Edelstein, Phys. Rev. Lett. **75**, 2004 (1995).
 - [2] L. P. Gor'kov and E. I. Rashba, Phys. Rev. Lett. **87**, 037004 (2001).
 - [3] P. A. Frigeri, D. F. Agterberg, A. Koga, and M. Sigrist, Phys. Rev. Lett. **92**, 097001 (2004).
 - [4] K. V. Samokhin, E. S. Zijlstra, and S. K. Bose, Phys. Rev. B **69**, 094514 (2004).
 - [5] I. A. Sergienko and S. H. Curnoe, Phys. Rev. B **70**, 214510 (2004).
 - [6] E. Bauer *et al.*, Phys. Rev. Lett. **92**, 027003 (2004).
 - [7] S. S. Saxena and P. Monthoux, Nature **427**, 799 (2004).
 - [8] E. Bauer, I. Bonalde, and M. Sigrist, to be published.
 - [9] G. Dresselhaus, Phys. Rev. **100**, 580 (1955).
 - [10] E. I. Rashba, Fiz. Tverd. Tela (Leningrad) **1**, 407 (1959), [Sov. Phys. Solid State **1**, 366 (1959)].
 - [11] L. N. Bulaevski, A. A. Guseinov, and A. I. Rusinov, Sov. Phys. JETP **44**, 1243 (1976).
 - [12] P. A. Frigeri, D. F. Agterberg, and M. Sigrist, New J. Phys. **6**, 115 (2004).
 - [13] M. Yogi *et al.*, Phys. Rev. Lett. **93**, 027003 (2004).
 - [14] E. Bauer *et al.*, cond-mat/0408244.
 - [15] R. P. Kaur, D. F. Agterberg, and M. Sigrist, cond-mat/0408149.
 - [16] P. A. Frigeri and M. Sigrist, in preparation.
 - [17] P. W. Anderson, Phys. Rev. B **30**, 4000 (1984).
 - [18] G. Eilenberger, Z. Phys. **214**, 195 (1968).
 - [19] A. I. Larkin and Yu. N. Ovchinnikov, Zh. Éksp. Teor. Fiz. **55**, 2262 (1968), [Sov. Phys. JETP **28**, 1200 (1969)].
 - [20] J. W. Serene and D. Rainer, Phys. Rep. **101**, 221 (1983).
 - [21] N. Schopohl, J. Low Temp. Phys. **41**, 409 (1980).
 - [22] C. T. Rieck, K. Scharnberg, and N. Schopohl, J. Low Temp. Phys. **84**, 381 (1991).
 - [23] C. H. Choi and J. A. Sauls, Phys. Rev. B **48**, 13684 (1993).
 - [24] H. Kusunose, Phys. Rev. B **70**, 054509 (2004).
 - [25] V. P. Mineev, Int. J. Mod. Phys. B **18**, 2963 (2004), cond-mat/0406371.
 - [26] N. Hayashi and Y. Kato, Physica C **388-389**, 513 (2003).
 - [27] S. Fujimoto, cond-mat/0503318.